Using the Rodrigues formula, the first term of (11) becomes:

$$\| -(n-1)P_0$$
$$+(1-\cos(\theta))(\hat{n}\cdot P_1)\hat{n} \quad +\cos(\theta)P_1 \quad +\sin(\theta)(\hat{n}\times P_1)$$
$$+(1-\cos(2\theta))(\hat{n}\cdot P_2)\hat{n} \quad +\cos(2\theta)P_2 \quad +\sin(2\theta)(\hat{n}\times P_2)$$
$$\vdots \qquad \vdots \qquad \vdots$$
$$+(1-\cos((n-1)\theta))(\hat{n}\cdot P_{n-1})\hat{n}+\cos(n-1)\theta)P_{n-1}+\sin(n-1)\theta)(\hat{n}\times P_{n-1})\|^2$$

Denoting the vectors:

$$A_0 = -(n-1)P_0 + \cos(\theta)P_1 + \ldots + \cos((n-1)\theta)P_{n-1}$$
$$B_0 = (1-\cos(\theta))P_1 + \ldots + (1-\cos((n-1)\theta))P_{n-1}$$
$$C_0 = \sin(\theta)\,P_1 + \ldots + \sin((n-1)\theta)P_{n-1}$$

we obtain for the first term in (11):

$$\|A_0 + (\hat{n}\cdot B_0)\hat{n} + \hat{n}\times C_0\|^2$$

With similar expressions for all other terms, (11) can be written:

$$\sum_{j=0}^{m}\|A_j + (\hat{n}\cdot B_j)\hat{n} + \hat{n}\times C_j\|^2 \qquad (12)$$

We minimize (12) over all possible vectors n under the constraint $\|n\| = 1$. Using Lagrange multipliers we obtain the following nonlinear system of matrix equations:

$$Mn + H - \lambda n = 0$$
$$n^t n - 1 = 0$$

where M is the matrix: $\sum_{j=0}^{m}(B_jB_j^t + C_jC_j^t + A_jB_j^t + B_jA_j^t)$, H is the vector $\sum_{j=0}^{m}(C_j \times A_j)$, and λ is the Lagrange multiplier.

Several numerical methods are available for solving such nonlinear systems. We used a variant of the iterative Newton method. This method requires initial values which we chose as the principal axes of the object whose C_n symmetry we are measuring (iteratively solving the system for each principal axis and choosing the best solution).

C.2. Reflection-Symmetry. Given a set of vectors in 3D, P_0, ..., P_{m-1}, we assume $m = 2q$. For simplicity we assume that the division into q pairs of vertices (as described in Section 3.4) is such that every two consecutive vectors constitute a pair (i.e., $\{P_{2i}, P_{2i+1}\}$ for $i = 0...q-1$). We wish to find the reflective-symmetry transformation of these vectors. Given a reflection plane, $S(\sigma)$ is calculated (according to eq 7 and similar to the description given in Section 3.4 for the 2D case) by reflecting one vector from each pair across the reflection plane, averaging with the other vector of the pair, and reflecting back the obtained average vector (see also Figure 8). In the general case, where the reflection plane is not known a priori, a minimization process must be adopted to find the reflection plane that minimizes the symmetry distance. We chose a gradient descent method which incrementally changes the reflection plane so that the CSM value is decreased at each iteration. The process converges to the reflection plane minimizing the symmetry distance.

A New Look at an Old Ligand: Surprises with Thioethers. A Density Functional Study

Heiko Jacobsen, Heinz-Bernhard Kraatz, Tom Ziegler,* and P. Michael Boorman

Contribution from the Department of Chemistry, University of Calgary, 2500 University Drive N.W., Calgary, Alberta, Canada T2N 1N4. *Received December 10, 1991*

Abstract: Using approximate density functional theory (DFT), the electronic and geometrical structures of thioether-containing d^3–d^3 face-sharing bioctahedral complexes of the type $[Mo_2Cl_{9-n}(SH_2)_n]^{n-3}$, with n = 2, 3, 4, 5, and $(SH_2)Cl_2Mo(\mu\text{-}Cl)_2(\mu\text{-}SR_2)MoCl_2(SH_2)$, with R = H, F, CH_3, are studied. All structures have been partially optimized and are in good agreement with the experiment. The fact that a thioether possesses one lone pair less than chloride decreases the repulsive interaction within the bridge. This and the availability of an empty σ^* orbital on the thioether ligand are largely responsible for a remarkable shortening of the Mo–Mo bond. All $(\mu\text{-}Cl)_3$ complexes exhibit a high-spin configuration with a long Mo–Mo distance (282 pm–268 pm), whereas the systems with one or more SR_2 ligands in the bridge has a low-spin configuration with a short Mo–Mo bond (256 pm–246 pm). The spin-coupling constant J_{ab}[Ia] of the antiferromagnetic complex $[(SH_2)Cl_2Mo(\mu\text{-}Cl)_3MoCl_2(SH_2)]^-$ (Ia) has been calculated to be -385 cm^{-1}, in close agreement with experimental coupling constant for related systems. Fragment analysis shows that the largest contribution to bonding clearly stems from σ donation of electron density from the sulfur's lone pairs (p_x and sp-hybrid). The σ-donor strength increases as follows: $S(CH_3)_2 > SH_2 > SF_2$. However, back-donation from the metal centers to a vacant σ^* orbital of the bridging thioether represents a sizable portion of the overall bonding energy. Expectedly, the π-acceptor ability of thioethers increases upon an increased electronegativity of the substituent on the thioether. Back-bonding is of lesser importance for terminal thioethers.

1. Introduction

A proper description of unsupported metal–metal bonds in naked dimers as well as binuclear complexes has been one of the more intriguing challenges to modern computational chemistry concerned with electronic structure theory. Intense scrutiny has been given to the hextuple bonded M_2 (M = Cr, Mo, W) dimers[1-5] as well as the quadruple[3,6-10] and triple bonded[11] binuclear complexes of the chromium triad. Many of the difficulties originate from the presence of σ- as well as π- and δ-bonds with vastly different requirements in terms of electron correlation. The computational problems are compounded further by the need to give a proper description of the relative involvement from the rather diffuse s-type orbitals as well as the more contracted d orbitals. It is still far from routine to provide a quantitative

(1) Delley, B.; Freeman, A. J.; Ellis, D. E. *Phys. Rev. Lett.* **1983**, *50*, 488.
(2) Baycara, N. A.; McMaster, B. N.; Salahub, D. R. *Mol. Phys.* **1984**, *52*, 891.
(3) Ziegler, T.; Tschinke, V.; Becke, A. *Polyhedron* **1987**, *6*, 685.
(4) Goodgame, M. M.; Goddard, W. A., III *Phys. Rev. Lett.* **1985**, *54*, 661.
(5) Bursten, B. E.; Cotton, F. A.; Hall, M. B. *J. Am. Chem. Soc.* **1980**, *102*, 6348.
(6) Ziegler, T. *J. Am. Chem. Soc.* **1984**, *106*, 5901.
(7) Ziegler, T. *J. Am. Chem. Soc.* **1985**, *107*, 4453.
(8) Benard, M.; Wiest, R. *Chem. Phys. Lett.* **1985**, *122*, 447.
(9) Hall, M. B. *Polyhedron* **1987**, *6*, 679.
(10) Bursten, B. E.; Clark, D. L. *Polyhedron* **1987**, *6*, 695.
(11) Ziegler, T. *J. Am. Chem. Soc.* **1983**, *105*, 7543.

0002-7863/92/1514-7851$03.00/0

Table I. Some Structural Data of Molybdenum–Thioether Complexes Possessing a Face-Sharing Bioctahedral Framework

compound		d_{M-M}, pm	β_1, deg	β_2,[b]	α',[b] deg
$[PPh_4][(Me_2S)Cl_2Mo(\mu\text{-}Cl)_3MoCl_2(Me_2S)$	I	274.6	68.2	68.4	89.1
$(THT)Cl_2Mo(\mu\text{-}Cl)_3MoCl(THT)_2$[a]	II	268.9	66.3	66.2	92.2
$(Me_2S)Cl_2Mo(\mu\text{-}Cl)_2(\mu\text{-}SMe_2)MoCl_2(Me_2S)$	III	246.2	61.6	59.7	100.5
$(THT)Cl_2Mo(\mu\text{-}Cl)_2(\mu\text{-}THT)MoCl_2(THT)$[a]	IV	247.0	61.8	59.7	99.1

[a] THT = tetrahydrothiophene. [b] Average value.

account of the unsupported metal–metal bond.

Supported metal–metal bonds bridged by ligands represent perhaps an even more formidable computational challenge.[12,13] The metal–metal bond in bridge complexes exhibit all the intricacies found in unsupported systems and encompass in addition a delicate balance between metal–ligand and metal–metal interactions. Thus, the replacement of a single ligand in the bridge can drastically change the length and electronic structure of the supported metal–metal bond. We shall in the following demonstrate how density functional theory[13] is able to account quantitatively for the dichotomies between the electronic and molecular structure of chloro-bridged bioctahedral complexes (I, II) and of their thioether-bridged analogues (III, IV). We shall further illustrate how the same theory can provide qualitative insight into the characteristics of different groups as ligands in terminal and bridging positions.

Previously, we reported on the syntheses and structures of some chloro-bridged bioctahedral complexes (I, II) and of their thioether-bridged analogues (III, IV) (see Table I).[14,15] It is evident that the massive structural changes observed are closely related to the nature of the bridging ligand. The bridging thioether causes a strong interaction of the two molybdenum centers, as is indicated by the shortening in the Mo–Mo bond length and by a change in magnetic behavior of the complexes. In order to understand the influence of the bridging thioether, we turned our attention to the literature to see what was known for thioether–transition metal bonding in general.

The bonding situation for thioether complexes is less than clear and is mainly based on experimental evidence. In IR studies, Cotton and Zingales[16] found that thioethers increase the stretching frequencies of CO in substituted metal-based carbonyl species more than N-based but less than P-based ligands. Various authors[16,17] ascribe this to differences in the strength of π-back-bonding, according to which thioethers are to be placed between amines and phosphines. The variety of experiments which all give support for back-bonding in thioether complexes includes X-ray investigations,[18,19] UV studies on crown thioether complexes,[20] and photoelectron spectroscopy on thioether substituted chromium carbonyl[21] as well as electrochemical studies on Os and Ru complexes,[22] EPR, and magnetic measurements.[23,24]

The above poses a question as to the nature of the bonding in thioether complexes. It is widely accepted that thioethers are weakly bound ligands, because they are weak σ donors and weak π acceptors.[25-27] The common and conventional explanation of

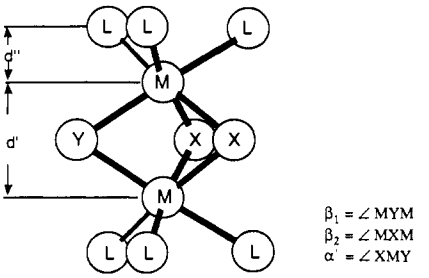

Figure 1. A general confacial bioctahedron. The structural parameters are defined according to Cotton and Ucko.[37]

back-bonding for third-row elements makes use of the fact that they possess empty 3d orbitals, which might have the right symmetry and energy to undergo additional bonding interactions.[28,29] Although this is a fruitful concept, it still is to be looked at as a heuristic model. In most cases, the real bonding situation is more delicate and needs more careful investigation both from the experimental as well as from the theoretical point of view.

A classical example illustrating this point can be seen in tertiary phosphines R_3P which have traditionally been regarded as good π-acceptor ligands due to their empty 3d orbitals.[30,31] However, theoretical studies by Trogler[32] and by Marynick[33] showed that these orbitals are too high in energy to reasonably interact with a metal center. It is suggested that P–R σ^* orbitals function as the acceptor orbitals instead. Prompted by these calculations, Orpen and Connelly[34] presented structural evidence for back-donation into P–R σ^* orbitals. It still remains to be seen whether this concept applies to thioethers as well.[35]

Among the various structural types of ligand bridged transition metal systems, many compounds containing thioethers prefer the confacial bioctahedral structure[36] (see Table I). This class of molecules has been the subject of various theoretical investigations,[37-41] mainly concerned with the question of the metal–metal bonding. Cotton and Ucko[37] were first to introduce interdependent structural parameters (see Figure 1) to describe the distortion compared to an ideal bioctahedron and hence the strength of the metal–metal bond. A strong metal–metal interaction will cause the ration d'/d'' to be less than its ideal value of 2, β to be smaller than the ideal angle of 70.5°, and α to be larger than 90°.

(12) Benard, M. *Inorg. Chem.* **1987**, *26*, 4908.
(13) Labanowski, J., Andzelm, J., Eds. *Density Functional Methods in Chemistry*; Springer-Verlag: Heidelberg, 1991.
(14) Moynihan, K. L.; Gao, X.; Boorman, P. M.; Fait, J. F.; Freeman, G. K. W.; Thornton, P.; Ironmonger, D. J. *Inorg. Chem.* **1990**, *29*, 1649.
(15) Boorman, P. M.; Moynihan, K. J.; Oakley, R. T. *J. Chem. Soc., Chem. Commun.* **1982**, 889.
(16) Cotton, F. A.; Zingales, F. *Inorg. Chem.* **1962**, *1*, 145.
(17) Ainscough, E. W.; Birch, E. J.; Brodie, A. M. *Inorg. Chim. Acta* **1976**, *20*, 187.
(18) Baker, E. M.; Larsen, N. G. *J. Chem. Soc.* **1976**, 1769.
(19) Lappert, M. F.; Shaw, D. B.; McLaughlin, G. M. *J. Chem. Soc., Dalton Trans.* **1979**, 427.
(20) Cooper, S. R.; Rawle, S. R.; Hartman, J. R.; Hintsa, E. J.; Admans, G. A. *Inorg. Chem.* **1988**, *27*, 1209.
(21) Weiner, M. A.; Lattman, M. *Inorg. Chem.* **1984**, *17*, 1084.
(22) Root, M. J.; Sullivan, B. P.; Meyer, T. J.; Deutsch, E. *Inorg. Chem.* **1985**, *24*, 2731 (1985).
(23) Reinen, D.; Ozarowski, A.; Jakob, B.; Pebler, J.; Stratemeier, H. *Inorg. Chem.* **1987**, *26*, 4010.
(24) Hartman, J. R.; Hintsa, E. J.; Cooper, S. R. *J. Chem. Soc., Chem. Commun.* **1984**, 386.
(25) Livingston, S. E. *Q. Rev. Chem. Soc.* **1965**, *19*, 386.
(26) Murray, S. G.; Hartley, F. R. *Chem. Rev.* **1981**, *81*, 365.
(27) Cooper, S. R.; Rawle, S. C. *Struct. Bonding* **1990**, *72*, 1.
(28) Huheey, J. E. *Inorganic Chemistry*, 3rd ed.; Harper & Row: Cambridge, 1983; p 824 ff.
(29) Kuehn, C. G.; Isied, S. S. *Prog. Inorg. Chem.* **1980**, *27*, 153.
(30) Cotton, F. A.; Wilkinson, G. *Advanced Inorganic Chemistry*, 5th ed.; John Wiley: New York, 1988; p 64 ff.
(31) Collman, J. P.; Hegedus, L. S.; Norton, J. R.; Finke, R. G. *Principles and Applications of Organotransition Metal Chemistry*; University Science Books: Mill Valley, CA, 1987; p 66 ff.
(32) Xiao, S.-X.; Trogler, W. C.; Ellis, D. E.; Berkovich-Yellin, Z. B. *J. Am. Chem. Soc.* **1983**, *105*, 7033.
(33) Marynick, D. S. *J. Am. Chem. Soc.* **1984**, *106*, 4064.
(34) Orpen, A. G.; Connelly, N. G. *J. Chem. Soc., Chem. Commun.* **1985**, 1310.
(35) Blake, A. J.; Schröder, M. *Adv. Inorg. Chem.* **1990**, *35*, 2.
(36) Messerle, L. *Chem. Rev.* **1988**, *88*, 1229.
(37) Cotton, F. A.; Ucko, D. A. *Inorg. Chim. Acta* **1972**, *6*, 161.
(38) Summerville, R. H.; Hoffmann, R. *J. Am. Chem. Soc.* **1976**, *98*, 7240.
(39) Summerville, R. H.; Hoffmann, R. *J. Am. Chem. Soc.* **1979**, *101*, 3821.
(40) Trogler, W. C. *Inorg. Chem.* **1980**, *19*, 697.
(41) Jevzowska-Trzebiatowska, B.; Nissen-Sobocinska, B. *J. Organomet. Chem.* **1988**, *342*, 353.

Table II. Some Structural Data of Partially Optimized Molybdenum–Thioether Complexes Possessing a Face Sharing Bioctahedral Framework

$L_3Mo(\mu\text{-}X)(\mu\text{-}Y)MoL_3$			$d_{M\text{-}M}$, pm	$\beta_1^{(Y=Cl^-)}$	$\beta_1^{(Y=SR_2)}$	$\beta_2^{(X=Cl^-)}$	$\beta_2^{(X=SR_2)}$	$\alpha'^{(Cl^-,Cl^-)}$	$\alpha'^{(Cl^-,SR_2)}$	$\alpha'^{(SR_2,Cl^-)}$	$\alpha'^{(SR_2,SR_2)}$
$[(SH_2)Cl_2Mo(\mu\text{-}Cl)_3MoCl_2(SH_2)]^-$	Ia	C_{2v}	278.8	67.1°		64.9°		96.2°			
$(SH_2)Cl_2Mo(\mu\text{-}Cl)_3MoCl(SH_2)_2$	IIa	C_s	282.5	66.9°		67.3°		90.9°			
$(SH_2)Cl_2Mo(\mu\text{-}Cl)_2(\mu\text{-}SH_2)MoCl_2(SH_2)$	IIIa	C_{2v}	246.9		63.4°	55.0°				101.6°	
$(SH_2)Cl_2Mo(\mu\text{-}Cl)_2(\mu\text{-}SF_2)MoCl_2(SH_2)$	IVa	C_{2v}	249.5		67.1°	57.0°				99.8°	
$(SH_2)Cl_2Mo(\mu\text{-}Cl)_2(\mu\text{-}SMe_2)MoCl_2(SH_2)$	Va	C_{2v}	246.7		63.9°	56.8°				101.5°	
$[(SH_2)Cl_2Mo(\mu\text{-}SH_2)_2(\mu\text{-}Cl)MoCl_2(SH_2)]^+$	VIa	C_{2v}	252.7	59.7°			62.7°		98.3		
$[(SH_2)Cl_2Mo(\mu\text{-}SH_2)(\mu\text{-}Cl)(\mu\text{-}SH_2)MoCl_2(SH_2)]^+$	VIIa	C_s	250.0		62.8°	56.9°	62.0°			101.0°	98.1°
$[(SH_2)Cl_2Mo(\mu\text{-}SH_2)_3MoCl_2(SH_2)]^{2+}$	VIIIa	C_{2v}	256.6		64.8°		62.7°				96.8°

Similarly, a repulsive metal–metal interaction will show the opposite effects. Summerville and Hoffmann expanded those first important studies by using qualitative molecular orbital arguments and extended Hückel calculations.[38,39] In their fragment approach, two conical ML_3 fragments with a variety of terminal ligands, forming a M_2L_6 dimer, are interacted with an L_3-bridging fragment, using hydride, chloride, and carbonyl as representative bridging ligands. Depending on the electronic nature of the bridging ligands, compression or elongation of the metal–metal bond is expected. π acceptors like CO and pure σ donors like H^- will strengthen the metal–metal bond; π donors like Cl^- or SR^-, on the other hand, will lead to an elongation of the complex due to repulsive orbital interaction. Finally, the question of superexchange in d^3–d^3 metal–metal bonded dimers gave rise to several studies. Hay and co-workers[42] presented a general treatment of orbital interactions in metal dimer complexes in terms of the extended Hückel method. More detailed calculations on the classical system $[Mo_2Cl_9]^-$ were done by Stranger[43,44] and by Ginsberg,[45] who determined the exchange coupling constant J_{ab} by making use of the Xα-scattered wave method.

Rather than dealing exclusively with metal–metal bonding in bioctahedral complexes, we have tried to focus our attention on the ligand side of the problem. We chose to compare the thioether ligand to its group 17 neighbor Cl^-, which does not possess any empty σ^* orbitals. The starting point was found in the bioctahedral complexes $[PPh_4][(Me_2S)Cl_2Mo(\mu\text{-}Cl)_3MoCl_2(SMe_2)]$ (I) and $(Me_2S)Cl_2Mo(\mu\text{-}SMe_2)(\mu\text{-}Cl)_2MoCl_2(SMe_2)$ (III). Since large differences in structural and magnetic properties are observed, we expected significant discrepancies in the bonding situation for these ligands in the bridging position.

Over the last decade, approximate density functional theory (DFT) has proven to be a useful tool in molecular energetics and dynamics.[46] This is true especially in the field of transition metal chemistry.[47] The interested reader is referred to a multitude of recent review articles and monographs discussing in detail the theoretical approach, as well as the applications of DFT.[13,46,47,83,84] We have used DFT to elucidate the electronic and structural properties of face-sharing bioctahedral complexes containing thioether ligands. To examine the special bonding situation for the thioether ligand, we have calculated energies and geometries of d^3–d^3 binuclear complexes $[Mo_2Cl_{9-n}(SH_2)_n]^{n-3}$ with $n = 2$, 3, 4, 5 as well as on complexes $(SH_2)Cl_2Mo(\mu\text{-}Cl)_2(\mu\text{-}SR_2)\text{-}MoCl_2(SH_2)$ with R = H, F, Me. For the trichloro-bridged systems, we calculated the spin-coupling constant J_{ab}. Before presenting our results, we would like to discuss our DFT approach in more detail.

2. Computational Details

To get a first idea of the bonding situation for thioether ligands, calculations were performed on model systems containing SH_2 rather than SMe_2 or THT as ligands. This simplification will not significantly influence the general picture of thioether bonding. To study the effect of different SR_2 ligands in more detail, we introduced systems with modified thioether ligands in bridging position. Further it should be pointed out that all the systems under investigation were considered as d^3–d^3 species.

Molecular Orbital Calculations. All calculations were based on approximate density functional theory within the local density approximation.[48-50] The exchange scale factor, α_{ex}, was taken as 0.7. We used Stoll's potential[51,52] to correct for correlation of electrons with different spin. In addition, we used Becke's nonlocal exchange correction. Stoll's correction[51,52] in the parametrization of Vosko, Wilk, and Nusair (VWN)[55] was added self-consistently, whereas Becke's correction was added as a perturbation based on the density obtained from HFS + Stoll SCF calculation. Calculations on the spin-coupling constant J_{ab}[1] included as well inhomogenous gradient corrections for correlation due to Perdew.[56,57] The reported calculations were carried out utilizing the vectorized version of the HFS program system developed by Baerends et al.,[58,59] and vectorized by Ravenek.[60] The numerical integration was based on a scheme developed by Becke.[61]

A double-ζ STO basis[62,63] was employed for the *n*s and *n*p shells of the main group elements. For sulfur, this basis was augmented by a single 3d STO function, for hydrogen, we used a 2p STO as polarization. The *n*s, *n*p, *n*d, $(n + 1)$s, and $(n + 1)$p shells of molybdenum were represented by a triple-ζ STO basis. Electrons in lower shells were considered as core and treated according to the procedure due to Baerends et al.[58] A set of auxiliary[64] s, p, d, f, and g STO functions, centered on all nuclei, was used to fit the molecular density and present Coulomb and exchange potentials in each SCF cycle.

Bonding Energies and Energy Decomposition. All bonding energies were evaluated by the generalized transition state method due to Ziegler and Rauk.[65] This treatment also allows for a detailed energy decomposition of the total bonding energy into steric and single orbital contributions.[66]

Geometry Optimization. The calculations were done in C_{2v} or in C_s symmetry, respectively. The symmetry was maintained during the process of geometry optimization. As a further simplification, the molecules under investigation were optimized only with respect to the metal atoms and the bridging atoms. The geometry optimization procedure was based on a method developed by Versluis and Ziegler.[67]

Calculation of the Spin-Coupling Constant. The spin-coupling constant J_{ab} was calculated according to the method developed by Noodleman.[68-70]

(42) Hay, P. J.; Thibeault, C.; Hoffmann, R. *J. Am. Chem. Soc.* **1975**, *97*, 4884.
(43) Stranger, R.; Smith, P. W.; Grey, I. E. *Inorg. Chem.* **1989**, *28*, 1271.
(44) Stranger, R. *Inorg. Chem.* **1990**, *29*, 5231.
(45) Ginsberg, A. P. *J. Am. Chem. Soc.* **1980**, *102*, 111.
(46) Ziegler, T. *Chem. Rev.* **1991**, *91*, 651.
(47) Ziegler, T. *Pure Appl. Chem.* **1991**, *63*, 873.
(48) Gunnarsson, O.; Lundquist, I. *Phys. Rev.* **1974**, *B10*, 1319.
(49) Gunnarsson, O.; Lundquist, I. *Phys. Rev.* **1976**, *B13*, 4274.
(50) Gunnarsson, O.; Johnson, M.; Lundquist, I. *Phys. Rev.* **1979**, *B20*, 3136.
(51) Stoll, H.; Pavlidou, C. M. E.; Preuss, H. *Theor. Chim. Acta* **1978**, *49*, 143.
(52) Stoll, H.; Golka, E.; Preuss, H. *Theor. Chim. Acta* **1978**, *55*, 29.
(53) Becke, A. *J. Chem. Phys.* **1986**, *84*, 4524.
(54) Becke, A. *J. Chem. Phys.* **1988**, *88*, 1053.
(55) Vosko, S. H.; Wilk, L.; Nusair, M. *Can. J. Phys.* **1980**, *88*, 2547.
(56) Perdew, J. P. *Phys. Rev.* **1986**, *B33*, 8822.
(57) Perdew, J. P. *Phys. Rev.* **1986**, *B34*, 7406 (erratum).
(58) Baerends, E. J.; Ellis, D. E.; Ros, P. *Chem. Phys.* **1973**, *2*, 41.
(59) Baerends, E. J. Ph.D. Thesis Frije Universiteit, Amsterdam, 1975.
(60) Ravenek, W. In *Algorithms and Applications on Vector and Parallel Computers*; Riele, H. J. J., Dekker, Th. J., van de Horst, H. A., Eds.; Elsevier: Amsterdam, 1987.
(61) Becke, A. *J. Chem. Phys.* **1988**, *88*, 2547.
(62) Snijders, J. G.; Baerends, E. J.; Vernoijs, P. *At. Nucl. Data Tables* **1982**, *26*, 483.
(63) Vernoijs, P.; Snijders, J. G.; Baerends, E. J. *Slater Type Basis Functions for the Whole Periodic System, Internal Report*; Frije Universiteit: Amsterdam, 1981.
(64) Krijn, J.; Baerends, E. J. *Fitfunctions in the HFS Method, Internal Report*; Frije Universiteit: Amsterdam, 1984.
(65) Ziegler, T.; Rauk, A. *Theor. Chim. Acta* **1977**, *46*, 1.
(66) Ziegler, T. *A General Energy Decomposition Scheme for the Study of Metal-Ligand Interactions in Complexes, Clusters and Solids*; NATO ASI, in press.
(67) Versluis, L.; Ziegler, T. *J. Chem. Phys.* **1988**, *88*, 322.

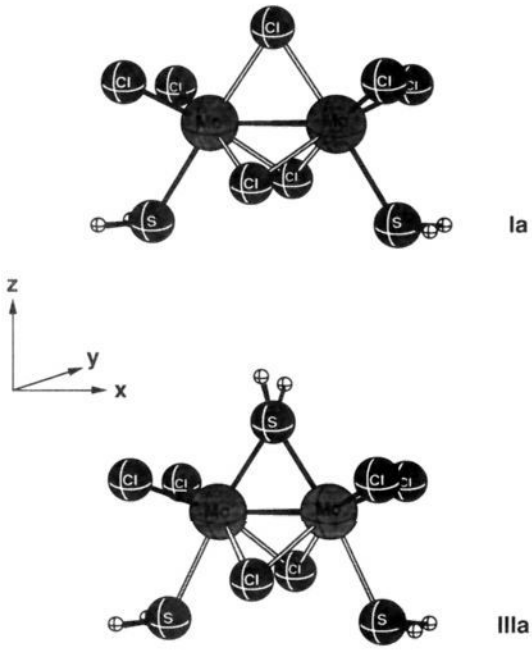

Figure 2. Optimized molecular structures of $[(SH_2)Cl_2Mo(\mu\text{-}Cl)_3MoCl_2(SH_2)]^-$ (**Ia**) and of $(SH_2)Cl_2Mo(\mu\text{-}Cl)_2(\mu\text{-}SH_2)MoCl_2$) (IIIa) in C_{2v} symmetry.

In the framework of DFT, this method allows for the calculation of J_{ab} from the energies of the highest spin state and a spin-polarized broken symmetry state.

3. Results and Discussion

We optimized the geometries of eight molybdenum thioether complexes. Compounds Ia, IIa, IIIa, VIa, and VIIIa have been calculated both as low-spin and as high-spin complexes. It turned out that the all-chloro-bridged complexes Ia and IIa possess a high-spin ground-state configuration, whereas all complexes, having one or more thioether ligands in the bridge, prefer the low-spin configuration. Table II displays theoretical structural data for the most stable states of these compounds. It is important to note the shorter Mo–Mo separation for all thioether-bridged complexes, ranging from 246.7 pm for Va to 256.6 pm for VIIIa. As a consequence, the angles α', β_1, and β_2 (see Figure 1) deviate significantly from their ideal values given in Cotton and Ucko's description.[37]

For our discussion, we shall distinguish between two types of bridging ligands X and Y as indicated in Figure 1. Y lies on the 2-fold axis of C_{2v} systems and is in a staggered conformation with the terminal Cl^- ligands. The other two bridging positions are then designated as X. For IIa the mirror plane maintained is the σ_{xz} plane. Thus the irreducible representations a_1 and b_1 of the point group C_{2v} correlate with a′ symmetry of C_s whereas a_2 and b_2 correlate with a″ symmetry. For VIIa the σ_{yz} plane is the mirror plane and we have correlations between a_1, b_2, and a′ as well as a_2, b_1, and a″, respectively.

Comparing the model structures Ia and IIIa (see Figure 2) with the related compounds I and III, we find that the calculated bond distances are, within differences of 2 pm and 0.5 pm, in good agreement with the experiment.[14,15] Further the angles β_1 could be calculated within a range of ±2°. This angle is less sensitive to the introduced simplification in the structure, since the bridging thioether possesses a staggered conformation with respect to the neighboring terminal chloro ligands. For the angles β_2 and α' these changes become more important, since steric interactions between the bridging chloro and the terminal sulfur ligands increase. However, it should be pointed out that the calculation satisfactorily

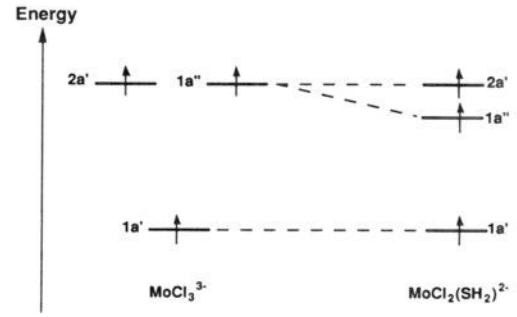

Figure 3. Schematic illustration of the energy splitting of the frontier orbitals of $MoCl_3^{3-}$ and of $MoCl_2(SH_2)^{2-}$.

represents the basic features of the experimental structures, that is, the metal–metal bond length, the characteristic angle β_1, as well as the magnetic behavior of different compounds.

Electronic Structure of Face-Sharing Bioctahedral Systems. In comparison with chloride, the thioether sulfur possesses only two lone electron pairs, namely, a p_x orbital (**1a**) and an sp_z hybrid

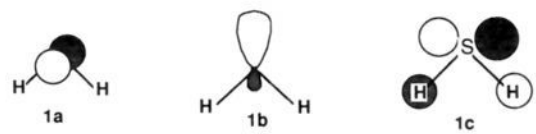

orbital (**1b**). However, in addition thioethers possess a vacant σ^* orbital (**1c**) with the same nodal characteristics as the additional lone pair on chloride.

To examine the influence of the thioether ligand in the bioctahedral framework, we have to look at the terminal ML_3 fragment first. We restrict ourselves to a frontier orbital discussion. For $MoCl_3^{3-}$, the singly occupied frontier orbitals are made up of a degenerate 2a′ (**2a**) 1a″ (**2b**) pair and a 1a′ combination (**2c**)

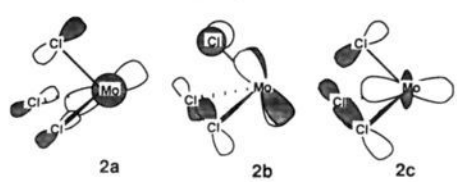

at lower energy. These three orbitals are essentially π-antibonding orbitals with respect to the metal–ligand interaction. On introducing thioether into the coordination sphere of the molybdenum the degeneracy of the 2a′ (**3a**) and 1a″ (**3b**) orbitals is removed.

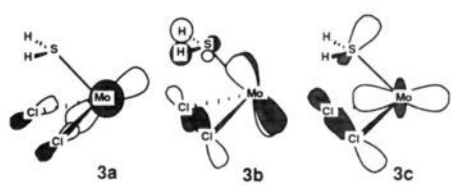

The thioether's lack of a lone pair, compared to chloride, and the accessibility of a low-lying and electron-accepting σ^* orbital are responsible for the decrease in energy of the 1a″ orbital (**3b**) (see Figure 3). The 2a′ (**3a**) and the 1a′ (**3c**) orbitals are essentially unaffected by the replacement of chloride by thioether.

Turning our attention to the electronic structure of $L_3M(\mu\text{-}X)_2(\mu\text{-}Y)ML_3$, we base our analysis on the Summerville and Hoffmann approach.[39] Rather than repeating their derivation, we want to summarize briefly the main features and adopt the analysis, originally performed for D_{3h} symmetry, for our systems in C_{2v} symmetry.

For Ia, the three bridging chloride ligands have in total nine fully occupied p orbitals. Their interaction with the set of M_2L_6-fragment orbitals results in three orbitals which are metal–metal bonding: $1a_1$ (**4a**), $1b_2$ (**4b**), and $2a_1$ (**4c**). With regard to the metal contribution, $1a_1$ is a linear combination of d_{z^2} and $d_{x^2-y^2}$ orbitals with about 25% $d_{x^2-y^2}$ character; it therefore rep-

(68) Noodleman, L.; Norman, J. G. *J. Chem. Phys.* **1979**, *70*, 4903.
(69) Noodleman, L. *J. Chem. Phys.* **1981**, *74*, 5737.
(70) Noodleman, L.; Baerends, E. J. *J. Am. Chem. Soc.* **1984**, *106*, 2316.

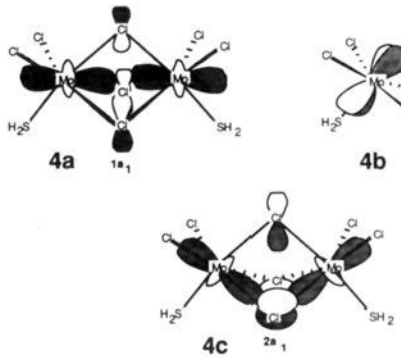

resents a metal–metal σ-bond. $2a_1$, on the other hand, is a linear combination of the same basis functions, but with major contributions from the $d_{x^2-y^2}$ orbitals resulting in a mostly δ-type orbital. $1b_2$ is a second mostly δ-type orbital, containing almost equal portions of d_{xy} and d_{yz} metal orbitals. Further we note that for the $1a_1$ orbital the interaction of the metal centers and the bridging ligands is strongly antibonding. The $1b_2$ and $2a_1$ orbitals show antibonding interaction only for the bridging ligand in the Y position. For the previously discussed $Mo_2Cl_9^{3-}$ molecule, these two orbitals are degenerate and form the e′ set of HOMOs (see Figure 4). It is evident from our short discussion of the ML_3 fragment that, upon introduction of thioethers into a terminal position in the bioctahedron, this degeneracy is lifted (see Figure 4).

The next two orbitals at higher energy, $1a_2$ (**4d**) and $1b_1$ (**4e**), are mainly metal based and destabilizing with respect to the Mo–Mo bond. In fact, $1a_2$ and $1b_1$ can be seen as the antibonding counterparts of $1b_2$ and $2a_1$, respectively. Other orbitals will be of minor importance for our discussion and will not be analyzed further.

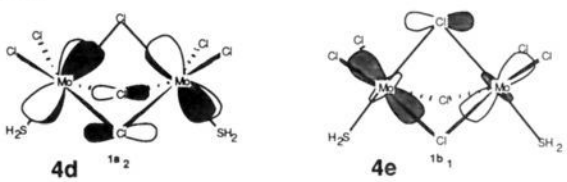

For the analogous thioether-bridged system $L_3M(\mu\text{-}X)_2(\mu\text{-}Y)ML_3$, X = Cl, Y = SH_2 (IIIa), again we consider only the five orbitals: $1a_1$ (**5a**), $1b_2$ (**5b**), $2a_1$ (**5c**), $1a_2$ (**5d**), and $1b_1$ (**5e**). Repeatedly we have been pointing out the lack of a lone pair on the thioether sulfur. This lack of a lone pair on sulfur in the Y position reduces the repulsive interaction between the bridge and the metal fragment. It is the $1b_2$ orbital only which gets significantly stabilized upon replacing chloride, **4b**, for thioether, **5b**. The other orbitals remain virtually unaffected. In fact, we find the antibonding Cl–Mo interaction in **4b** replaced by a bonding interaction in **5b** between a vacant σ^* orbital of the thioether, having the correct symmetry and a comparable energy, and the M_2L_6 fragment. The interaction between the σ^* orbital of the thioether and the metals' d orbitals is schematically shown in **5f**. The view is along the Mo–Mo vector. The orbital contributions from the remaining ligands has been omitted for the reason of clarity.

We can interpret this interaction as back-bonding from the occupied d orbital of the metals to the sulfur ligand. Hence, it is the $1b_2$ orbital that will be crucial to our further discussion. In Figure 4, the effect of the thioether substitution is shown. A terminal thioether leads to a removal in degeneracy of the e′ set of $Cl_3Mo(\mu\text{-}Cl)_3MoCl_3^{3-}$ giving rise to a $1b_2$ and a $2a_1$ orbital. The reason for this has been explained earlier as a secondary effect of the terminal thioether ligands on the ML_3 fragment (cf. Figure 3). The splitting between these two orbitals is increased dramatically by the introduction of the bridging thioether leading to a net stabilization of the $1b_2$ orbital.

In summary, we can say that it is the possibility of back-donation and the decrease of repulsive interactions between the

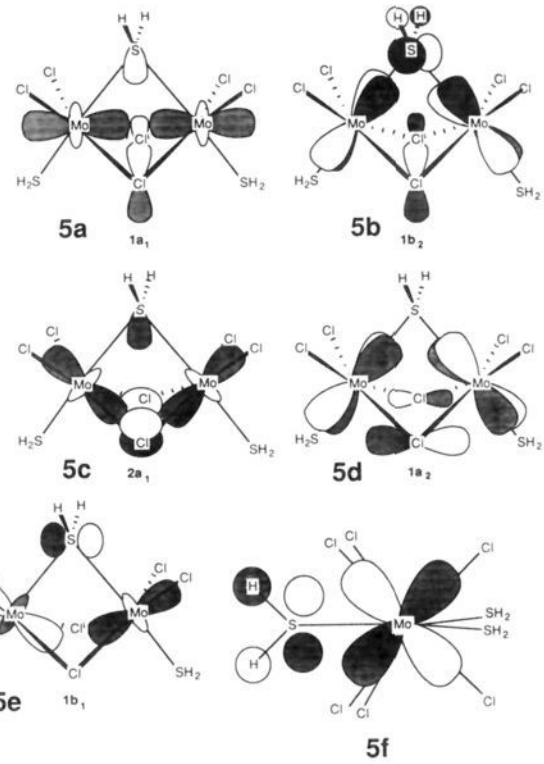

bridging ligands and the metal fragment which are the main features causing the difference in electronic structure of bioctahedral systems with and without bridging thioether ligands.

High-Spin Systems Versus Low-Spin Systems. Using the conclusion we have drawn so far, the explanation of the different geometries and spin states for $(\mu\text{-}Cl)_3$ and $(\mu\text{-}SH_2)(\mu\text{-}Cl)_2$ systems is straightforward. In order to compensate for the destabilizing interaction of bridging ligands and the metal centers, $(\mu\text{-}Cl)_3$ systems react with an elongation of the metal–metal bond. As the δ-type bonding orbitals become more and more nonbonding, only the metal–metal σ-bond is retained. Hence, the splitting of the orbitals $1b_2$, $2a_1$, $1a_2$, and $1b_1$ decreases; we obtain a set of four orbitals, which are close together in energy. This orbital configuration gives rise to high-spin systems. Figure 5 displays the frontier orbitals of Ia for optimized low-spin as well as high-spin geometries. For the low-spin case, the orbitals $1b_2$ and $2a_1$ are close together in energy. This emphasizes the fact that these two orbitals are degenerate in M_2Cl_9 systems. It is significant that the relative splitting between $1b_2$ and $2a_1$ increases from 0.146 eV in the low-spin configuration to 0.359 eV in the high-spin configuration. Again, the interactions between terminal thioether ligands and the bridge are dissimilar for a-type and b-type orbitals. It is indeed the fact that the exchange of terminal Cl^- against terminal SH_2 not only splits the degenerate e sets into a-type and b-type orbitals, but also causes different behavior of these orbitals under geometry distortions. We find for the high-spin case that the four frontier orbitals have energies between −1.615 eV and −2.160 eV. An electronic configuration of four unpaired electrons is therefore plausible.

Although a high-spin configuration is favorable for $(\mu\text{-}Cl_3)$ systems, Figure 5 indicates that in terms of orbital energy the low-spin case should be more stable than the high-spin case. However, it is important to keep in mind that the electronic interaction represents only one part of the total bonding interaction. It is the influence of the steric interaction which causes the high-spin state to be the more stable state. We will return to this point at the end of the following section, after we have introduced our energy decomposition scheme.

Introducing a bridging thioether ligand, the $1b_2$ orbital is supported by an empty σ^* orbital, which so to speak clamps the metal centers together, leading to strong interactions of the σ- and δ-type orbitals, respectively. Lengthening of the metal–metal

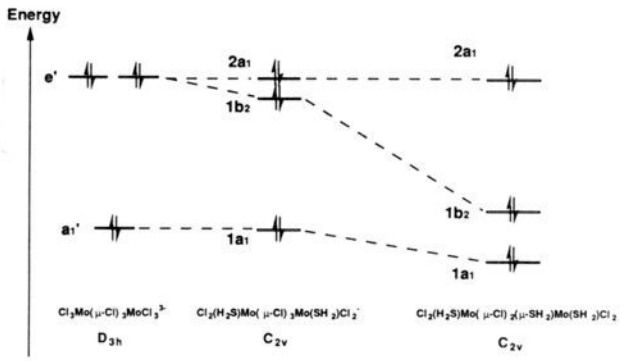

Figure 4. Schematic illustration of the energy splitting of the frontier orbitals of $[(SH_2)Cl_2Mo(\mu\text{-}Cl)_3MoCl_2(SH_2)]^-$ (Ia) and of $(SH_2)Cl_2Mo(\mu\text{-}Cl)_2(\mu\text{-}SH_2)MoCl_2(SH_2)$ (IIIa) compared to $[Cl_3Mo(\mu\text{-}Cl)_3MoCl_3]^{3-}$. The introduction of SH_2 first into a terminal position, and then into the bridging position, leads to successive stabilization of the $1b_2$ orbital.

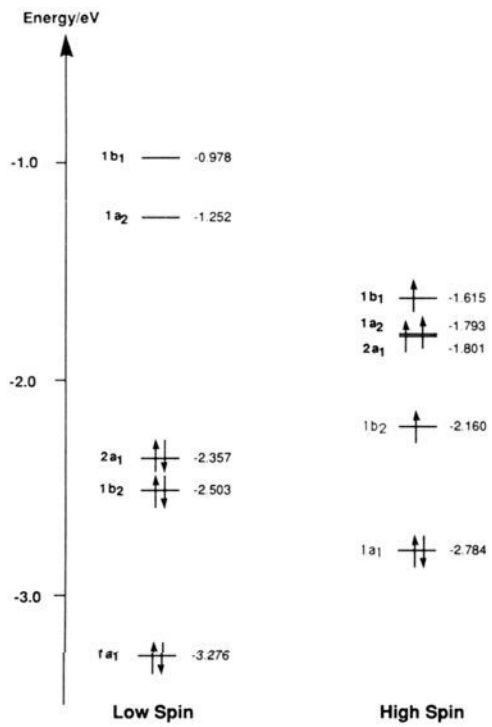

Figure 5. Energy level diagram of $[(SH_2)Cl_2Mo(\mu\text{-}Cl)_3MoCl_2(SH_2)]^-$ (Ia) for the optimized low-spin and high-spin geometries.

distance reduces the back-bonding, and, hence, it is no longer energetically favorable. Therefore, $(\mu\text{-}SH_2)(\mu\text{-}Cl)_2$ complexes have a short metal–metal bond and exhibit diamagnetic behavior. It can be seen in Figure 6 that for IIIa $1b_2$ and $2a_1$ are no longer close in energy. Now the situation is reversed, since in terms of energy the $1b_2$ orbital now approaches the $1a_1$ orbital. This clearly illustrates the stabilization of $1b_2$. Going to the high-spin system, it is remarkable that $2a_1$ now lies at higher energy than $1a_2$. Increasing the metal–metal distance destabilizes $2a_1$ by reducing the bonding overlap between the metal centers, but stabilizes $1a_2$ by reducing the antibonding overlap between the bridging ligand in the Y position and the metal centers. This compensation is more effective in $(\mu\text{-}Cl)_3$ than in $(\mu\text{-}SH_2)(\mu\text{-}Cl)_2$ systems, since Cl^- is the stronger σ donor. On the other side, $1a_2$ will decrease in energy, if we pull the metal centers apart. This explains the differences in changes for **2c** and **3c** and makes the orbital crossing attainable.

To support our calculations, we evaluated the spin-coupling constant for Ia. It is experimentally known that the complex I is antiferromagnetic and possesses a spin-coupling constant of $J_{ab}^{I} = -420\ cm^{-1}$.[14] Following the procedure introduced by Noodleman,[68-70] we found for our model complex Ia the spin-coupling constant to be $J_{ab}^{Ia} = -385\ cm^{-1}$. This result is in excellent agreement with the experiment.

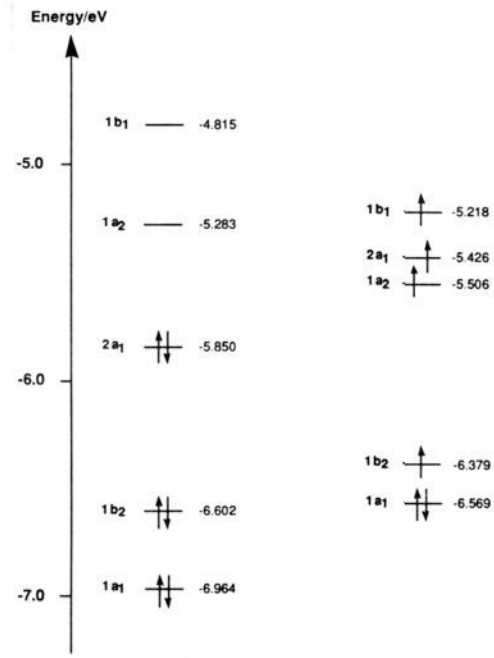

Figure 6. Energy level diagram of $(SH_2)Cl_2Mo(\mu\text{-}Cl)_2(\mu\text{-}SH_2)$ (IIIa) for the optimized low-spin and high-spin geometries. For the latter, the $1b_2$ orbital is well separated from the remaining set of singly occupied orbitals.

Scheme I

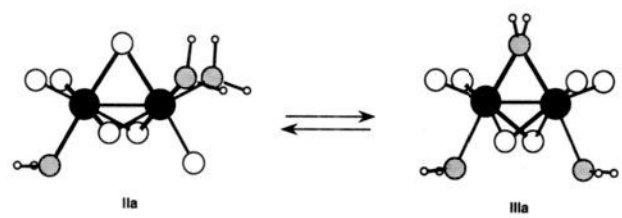

So far, we rationalized the different geometries and different spin states of our compounds under investigation. Of further interest is a detailed quantitative analysis of the bonding situation for the bridging ligands. The structures of isomers II and IV have been established experimentally. The exchange of a bridging Cl^- against a terminal THT ligand results in structural changes alluded to above. The question arises as to whether II or IV is the energetically more stable species.

We calculated the isomerization energy for the reaction $(SH_2)Cl_2Mo(\mu\text{-}Cl)_3MoCl(SH_2)_2$ (IIa) ↔ $(SH_2)Cl_2Mo(\mu\text{-}Cl)_2(\mu\text{-}SH_2)MoCl_2(SH_2)$ (IIIa) (Scheme I). We found the complex IIIa to be 11.6 kJ/mol more stable than IIa. As one might expect, the thioether bridged complex turned out to be the more stable. However, the small difference in the relative energies of IIa and IIIa might be somewhat of a surprise. To clarify the situation, we would like to present a more detailed bonding analysis, which not only considers electronic effects in terms of orbital interaction but also takes steric interactions into account.

Bond Analysis and Energy Decomposition. The generalized transition-state method provides not only accurate calculations of total bonding energies[65] but also the possibility of a detailed bonding analysis.[66,71,72] The reader is referred to the literature[66] for a detailed description and a list of applications of the transition-state method.

(71) Ziegler, T.; Rauk, A. *Inorg. Chem.* **1979**, *18*, 1558.
(72) Ziegler, T.; Rauk, A. *Inorg. Chem.* **1979**, *18*, 1755.

Table III. Bond Energies and Its Decomposition into Steric and Orbital Interaction for the Reaction $(H_2S)Cl_2Mo(\mu\text{-}Cl)_2MoCl_2(SH_2) + R \rightarrow (H_2S)Cl_2Mo(\mu\text{-}Cl)_2(\mu\text{-}R)MoCl_2(SH_2)$ with R = SH_2, SF_2, SMe_2, Cl^- [a]

		total bonding energy	steric interaction	orbital interaction
M_2L_8 [b] + SH_2	IIIa	−135.2	410.9	−546.1
M_2L_8 + SF_2	IVa	−200.8	638.9	−839.7
M_2L_8 + SMe_2	Va	−202.1	543.4	−745.5
M_2L_8 + Cl^-	Ia	−143.9	4.6	−148.5

[a] All energies are given in kJ/mol. [b] $M_2L_8 = (SH_2)Cl_2Mo(\mu\text{-}Cl)_2MoCl_2(SH_2)$.

Table IV. Decomposition of the Total Bond Energy into Contributions from Different Symmetries for the Reaction $(H_2S)Cl_2Mo(\mu\text{-}Cl)_2MoCl_2(SH_2) + R \rightarrow (H_2S)Cl_2Mo(\mu\text{-}Cl)_2(\mu\text{-}R)MoCl_2(SH_2)$ with R = SH_2, SF_2, SMe_2, Cl^-

		A_1, %	A_2, %	B_1, %	B_2, %
M_2L_8 + SH_2	IIIa	51.3	1.5	30.9	16.3
M_2L_8 + SF_2	IVa	40.9	2.7	31.3	25.1
M_2L_8 + SMe_2	Va	52.5	2.1	32.1	13.3
M_2L_8 + Cl^-	Ia	75.6	2.7	11.7	10.0

In order to investigate the chemical bonding of thioethers, we extended our calculations to $L_3M(\mu\text{-}X)_2(\mu\text{-}Y)ML_3$ systems with different thioethers in the Y position. The total energy for the reaction $(SH_2)Cl_2Mo(\mu\text{-}Cl)_2MoCl_2(SH_2) + R \rightarrow (SH_2)Cl_2Mo(\mu\text{-}Cl)_2(\mu\text{-}R)(\mu\text{-}SMe_2)MoCl_2(SH_2)$ with R = SH_2, SF_2, SMe_2, Cl^- can then be decomposed as

$$\Delta H_{LA} = -[\Delta E^0 + \Delta E_{el}] \quad (1)$$

where ΔE^0 represents the steric interaction energy between our M_2L_8 fragment and the ligand R, whereas ΔE_{el} combines the electronic contributions due to orbital interactions. We can define ΔH_{LA} as a ligand association energy. We should mention that (1) is already a simplification of the exact expression for ΔH_{LA}. We neglected the preparation energy ΔE_{prep} required to deform the single fragments from their equilibrium energy to the conformation in the final complex. Thus, ΔH_{LA} represents more closely a bond snapping energy. We can assume that for the thioether systems the preparation energy is of the same order of magnitude, so that we can satisfactorily assign the relative bond strength of these systems with respect to each other. Table III displays the results of a decomposition for the model systems Ia, IIIa, IVa, and Va. The most stable complexes are formed with SMe_2 and SF_2 in the bridging position. The energies for the bonding of SH_2 and Cl^- are about 65 kJ/mol and 55 kJ/mol less, respectively. Surprisingly, the Cl^- ligand undergoes stronger bonding with the M_2L_8 fragment than the SH_2 ligand. To explain this trend, we first focus on the thioether-bridged systems and begin with a discussion of the electronic effects.

The main difference in the bonding for the three thioether systems can be ascribed to the distinct orbital interactions and therefore can be analyzed in terms of electronic contributions. The term ΔE_{el} represents the main features of the common theory by Parr and Pearson,[73,74] in which the bond energy is related to differences in electronegativity and hardness between interacting fragments. The underlying idea is that the stability of a bond between two fragments is related to the gain in energy associated with the transfer of charge from one fragment to the other. In order to perform such a bonding analysis, we break down ΔE_{el} into different symmetry contributions. In Table IV, for our thioether systems, contributions from A_1 (**6a**) and B_1 (**6b**) are associated with donation; B_2 (**6c**) represents back-donation.

The contributions from A_2 are negligible. We can identify the most dominant interaction to be the donation from the sulfur lone pairs to the metal fragment, **6a**. For the SH_2 and SMe_2 ligands,

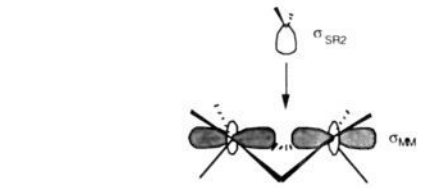

6a

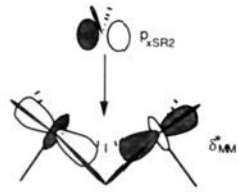

6b

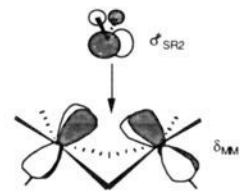

6c

this donation contributes with about 50% to the total bonding interaction. Further, we have contributions due to back-bonding from the metal fragment to the sulfur ligand, **6c**. With participations of 13.3% for SMe_2 and 16.3% for SH_2, the back-bonding is not the dominant interaction, but still represents a remarkable portion of the total bonding energy. It is mainly a σ^* orbital at the sulfur ligand, which is involved in back-donation. d orbitals, introduced as polarization functions, contribute with about 15–20% to the SR_2 b_2 orbital involved in back-bonding. Clearly, it is no single, empty d orbital, which is solely responsible for the back-bonding. When fluorine is introduced in the sulfur system, this strongly electronegative substituent increases the contribution of back-bonding up to 25.1%, and lessens the ability for σ donation, for which the contribution decreases to 40.9%. Using common theories such as the HSAB concept alluded to above, we could develop a similar, but only qualitative description of the bonding/back-bonding abilities of the SR_2 ligands.

Lastly, we have to consider another significant bonding interaction, that is, donation from a sulfur p orbital to the metal fragment, **6b**. For all of the SR_2 systems under investigation, this additional donation contributes about 30% to the main bonding interaction. The aforesaid leads us to conclude that thioethers have to be looked at as mainly σ donors with low π-accepting capacities. Only in systems with highly electronegative substituents at the sulfur does this back-bonding become of major importance.

We now compare the bonding of thioethers with the bonding of the Cl^- ligand. According to Table IV, as for the thioether ligand, the main interaction for Cl^- is the A_1 donation, from the p_z orbital of the incoming ligand to the metal system as shown in **6d**. However, this contribution now represents as much as

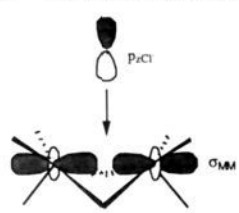

6d

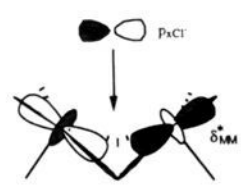

6e

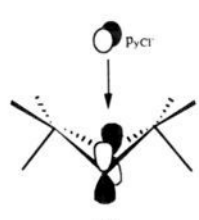

6f

three-quarters of the total interaction energy. Furthermore, it is of significance that the second donation from the chloride's p_x

(73) Pearson, R. G. *Inorg. Chem.* **1988**, *27*, 734.
(74) Parr, R. E.; Pearson, R. G. *J. Am. Chem. Soc.* **1983**, *105*, 7512.

Table V. Occupation of $Q(\sigma)$, $Q(\pi)$, and $Q(\sigma^*)$ for the SH_2 Orbitals 1a, 1b, and 1c, As Well As for the Related Orbitals of SF_2 and SMe_2, Obtained by Mulliken Population Analysis

	SH_2	SF_2	SMe_2
$Q(\sigma)$	1.75	1.88	1.69
$Q(\pi)$	1.71	1.52	1.57
$Q(\sigma^*)$	0.25	0.50	0.22

orbital to the metal system, the B_1 donation illustrated in **6e**, contributes only about 12% to the total interaction energy, whereas for the thioethers the similar interaction is about three times as high. The main reason here is the longer metal–metal distance in the Cl^- system, which consequently leads to a longer distance between the bridging ligand and the metal atoms. Since in the case of the B_1 donation the interaction between the bridging ligand and the metal system is oriented directly toward the two metal atoms and not as in the A_1 case toward the center of the metal atoms, an elongation of the metal–metal bond reduces the overlap between the bridging ligand and the metal system. This is reflected by the fact that the B_1 donation is only of minor importance for the Cl^- ligand.

The contributions in the A_2 representation are, as in the thioether case, negligible. The B_2 interaction is in contrast to the case of thioethers not a back-bonding interaction and contributes about 10% to the total interaction energy. We already mentioned that the interaction of the p_y orbital of Cl^- with the metal atoms is strongly repulsive. On the other hand, the incoming Cl^- can interact in a bonding fashion, **6f**, with the other two bridging ligands which gives rise to additional stabilization. However, compared to the A_1 donation, this bonding interaction is also of minor importance. In summary, we can say that in the systems under investigation the Cl^- ligand proves to be a classical σ donor.

Another way of looking at the chemical bonding involves population analysis. Table V displays occupations for several SR_2 orbitals of IIIa, IVa, and Va, obtained by a Mulliken population analysis. $Q(\sigma)$ represents the population in the donating a_1 orbitals, **6a**, $Q(\pi)$ represents the population in the donating b_1 orbitals, **6b**, and $Q(\sigma^*)$ is the charge donated back into the b_2 orbitals (**6c**). According to Table V, we find the following order for σ-donor strength: $SMe_2 > SH_2 > SF_2$. The opposite order will be obtained by classifying the ligands with respect to their acceptor ability. It is further notable that an important amount of charge is donated back to the sulfur ligand, up to 0.5 electron for SF_2. For the π donation, we find that SF_2 and SMe_2 are much better donors than SH_2. In the latter case, the donation is exclusively due to the single p orbital at the sulfur, **1a**. For the first two ligands we have additional antibonding contributions from p orbitals of the fluorine substituents as well as from appropriate combinations of hydrogen s orbitals of the metal group, as indicated in **7a** and **7b**.

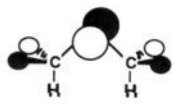

7a

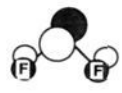

7b

By donating electrons to the metal system, the electron density at the sulfur is reduced and therefore also the antibonding interaction between the sulfur and its substituents. We conclude that not only the electronegativity of the substituents at SR_2 determines the bonding ability of the ligand, but also secondary influences due to additional orbital interactions.

Finally, we will include steric effects in our discussion. Above, we introduced the term ΔE^0, which denotes energy contribution due to steric interaction. ΔE^0 can be written as

$$\Delta E^0 = \Delta E_{elst} + \Delta E_{dlxc} + \Delta E_{exrp} \quad (2)$$

The electrostatic term ΔE_{elst} and the change in the exchange correlation energy ΔE_{dlxc} are in general stabilizing, whereas the exchange repulsion energy ΔE_{exrp} is the mainly destabilizing component of ΔE^0.[66] ΔE_{exrp} is directly related to the so-called "four-electron two-orbital" interactions. We see, from Table III, that for the sulfur ligands the trends in orbital interactions and steric interactions are correlated. As the orbital interaction increases, the distance between metal fragments and SR_2 ligand decreases, which induces a stronger destabilizing steric interaction.

The interesting result is, however, that for Cl^- in a bridging position the steric interaction is almost negligible. One of the reasons for this is certainly the larger metal–metal distance in Ia. The net result is that Cl^-, in spite of its smaller orbital interaction, by a factor of 3.5, surpasses SH_2 in overall bonding strength.

We now shall return to the isomerization reaction $(SH_2)Cl_2Mo(\mu\text{-}Cl)_3MoCl(SH_2)_2$ (IIa) $\leftrightarrow$ $(SH_2)Cl_2Mo(\mu\text{-}Cl)_2(SH_2)MoCl_2(SH_2)$ (IIIa) (Scheme I). To account for the small isomerization energy, the key point is not whether SH_2 or Cl^- holds the bridging Y position, since we have seen that the bonding energies for both cases are comparable, with preference for Cl^-. It is rather important to address the question of energy differences between terminal and bridged thioethers.

Because of the longer metal–ligand distance, both the electronic as well as the steric contributions are significant smaller for SH_2 in a terminal position. The decomposition analysis for IIIa shows the bonding energy for a terminal SH_2 ligand to be −82.9 kJ/mol. It is therefore 52.3 kJ/mol less stable than the bridging thioether. The contribution due to back-bonding decreases from 16.3% for the bridging case to 10.8% for the terminal case. Furthermore, we have to take into account the contributions from the chloride ligand. We recall that we form a less stable bond if we substitute SH_2 by Cl^- into the bridging position. The difference in energy between the terminal and bridging position is less significant for Cl^-. Using the isomerization energy for the process discussed in Scheme I and the bonding analysis for bridging ligands, we found the bonding energy for terminal chloride to be −101.2 kJ/mol. Cl^- is to be considered solely as a σ donor. The bonding interaction for a bridging chloride is increased by 42% with respect to a terminal chloride. For a bridging SH_2 the bonding energy is increased by 68% compared to a terminally bonded thioether. In both cases, the chloride is bonded more strongly to the metal fragment than SH_2. It is the larger increase in the bond energy of the bridging thioether that can be used to rationalize the small difference in energy between compounds IIa and IIIa, with IIIa being the thermodynamically more stable complex.

This section is concluded with a bond analysis of the $(\mu\text{-}Cl_3)$ system Ia, optimized for different spin states. Recalling that the change in the metal–metal distance is the most important geometrical difference in these complexes, it was seen that an elongation of the metal–metal bond makes a high-spin configuration plausible, but leads to an overall decrease in terms of the electronic interaction energy ΔE_{el} of eq 1. The elongation, on the other hand, will lead to a decrease in steric interaction, mainly due to a reduced exchange repulsion term. The difference in the change of the stabilizing electronic interaction energy, ΔE_{el}, and the destabilizing steric energy, ΔE^0, determines the geometry of Ia. Figure 7 illustrates the trends for Ia in the spin states $S_{max} = 0, 1, 2$. The low-spin singlet geometry ($S_{max} = 0$) has been optimized with a metal–metal bond distance of 228.6 pm. This corresponds to a strong coupling of the two metal centers. In-phase combinations of the three relevant metal d orbitals are formed and each is occupied with one pair of electrons. These orbitals are shown in **4a–c** and are designated as $1a_1$, $1b_2$, and $2a_1$. Besides the strong coupling of the two metal centers, two different possibilities of realizing weakly coupled systems have been considered. In the case where one electron pair is weakly coupled ($S_{max} = 1$), in-phase combinations of two d orbitals on each metal center are formed and each assigned with one electron pair. This leads to the formation of the orbitals $1a_1$ (**4a**) and $1b_2$ (**4b**). The third pair is described by two different orbitals for the α and β electrons, with one orbital polarized on the metal center A and the other one on the metal center B. These orbitals are asymmetric linear combinations of the third set of d orbitals. On going from the system with $S_{max} = 0$ to a system with $S_{max} = 1$, the metal–metal bond distance increases to 267.8 pm. The steric interaction and the orbital energy terms follow the expected trends. The overall energetic balance favors the singlet ($S_{max} = 0$) over the triplet

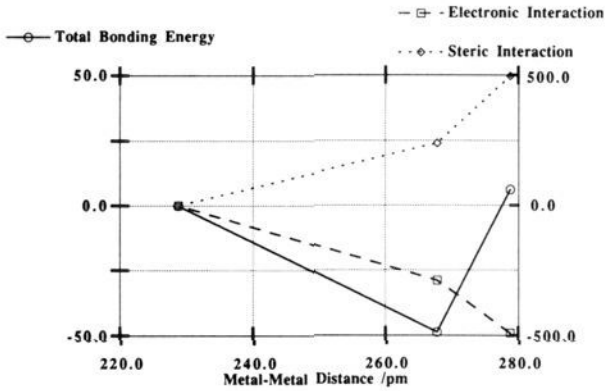

Figure 7. Electronic and steric contributions, ΔE_{el} and ΔE^0, to the total bonding energy for Ia in different spin states. The metal–metal distances of 228.0 pm, 267.1 pm, and 278.8 pm correspond to spin states S_{max} = 0, 1, 2, respectively. The energetic contributions for $S_{max} = 0$ are set to zero for clarity. Negative energies refer to destabilization. Note the double ordinate representation with a scale from −50 to 50 kJmol^{-1} for the total bonding energy and a scale from −500 to 500 kJmol^{-1} for the relative steric and electronic contributions.

state (S_{max} = 1) by about 50 kJ/mol.

For the two weakly coupled electron pairs (S_{max} = 2), both d orbitals on the metal center which give rise to δ-bonding are treated differently for electrons of different spins. The two electrons of α-spin are polarized toward center A and the two electrons of β-spin polarized toward center B. For the quintet high-spin state we find a metal–metal distance of 278.8 pm. The gain in energy due to the reduced steric interaction can overcompensate for the loss of energy due to the electronic interaction. It is remarkable that the energy difference between the low-spin state (S_{max} = 0) and quintet high-spin state (S_{max} = 2) amounts to only 6.1 kJ/mol. This indicates the fine balance and equal importance of steric as well as electronic effects for a proper bond description. The theory of Heisenberg spin coupling can result in a ferromagnetic coupling (J_{ab} is positive) or in antiferromagnetic coupling (J_{ab} is negative). For Ia, we find antiferromagnetic coupling in agreement with the experiment.[14] However, our theory must then lead to a singlet ground state, which should be about 30 kJ/mol more stable than the quintet state, whereas experimental results[14] indicate a triplet state to be the ground state. Only a configuration interaction treatment between all possible spin states of S_{max} = 2 with the same S = 0, 1, 2 can lead to the correct result. Such a treatment is not possible within the DFT formalism.

For the thioether-bridged systems, we find that the low-spin state (S_{max} = 0) is clearly preferred over the high-spin state (S_{max} = 2) by 31.2 kJ/mol. As we discussed above, this can be rationalized according to the different bonding behavior of thioether systems.

Systems Bridged by More Than One Thioether Ligand. The last point of our discussion deals with the multiple thioether effect, which is the influence of additional thioether ligands in the bridging position. $L_3M(\mu\text{-}SR_2)_n(\mu\text{-}Cl)_{3-n}ML_3$ compounds with n = 2, 3 are yet not known for molybdenum, but are well established for the tungsten systems.[75,76]

Figure 8 displays the energy level diagram for the frontier orbitals of IIIa, VIIa, and VIIIa, which all have one SH_2 ligand in the Y position and zero, one, and two SH_2 ligands in position X, respectively. The orbitals $1a_1$, $1b_2$, $1a_2$, $1b_1$, and their a′ and a″ analogues show a similar energy level pattern for all three complexes. It is the orbital $2a_1$ or 3a″, respectively, which is significantly stabilized by introducing additional thioethers in the position X of the bridge.

If we look at the contributions of the bridging orbitals separately, we find for the orbitals $1a_1$ and $1b_2$ that an SH_2 ligand

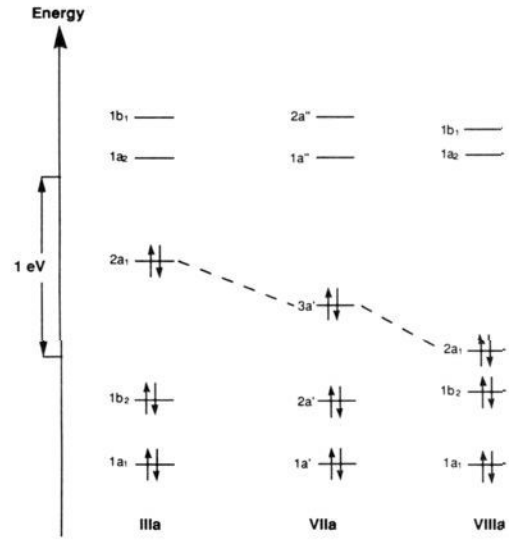

Figure 8. Energy level diagram of $(SH_2)Cl_2Mo(\mu\text{-}Cl)_2(\mu\text{-}SH_2)MoCl_2(SH_2)$ (IIIa), $(SH_2)Cl_2Mo(\mu\text{-}SH_2)(\mu\text{-}Cl)(\mu\text{-}SH_2)MoCl_2(SH_2)$ (VIIa), and $(SH_2)Cl_2Mo(\mu\text{-}SH_2)_3MoCl_2(SH_2)$ (VIIIa) in illustration of the multiple thioether effect.

in an X position does not participate in the formation of the overall bridging orbital. These orbitals are shown in **8a** and **8b** for the

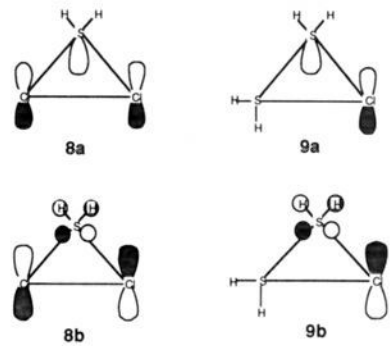

$(\mu\text{-}Cl)_2(\mu\text{-}SH_2)$ bridge and in **9a** and **9b** for the $(\mu\text{-}SH_2)(\mu\text{-}Cl)(\mu\text{-}SH_2)$ bridge. For **8a**, substitution of Cl^- for SH_2 to form **9a** leads to a stabilization of the bond between the ligand bridge and the metal fragment. On the other hand, the bonding in the bridge itself is weakened, since all three ligands interact in a bonding fashion. The same is true for the $1b_2$ orbitals **8b** and **9b** so that the relative energy of $1b_2$ with respect to $1a_1$ is about the same in all three complexes. For the 3a′ orbital of VIIa, the situation is different. Now the sulfur ligand participates with a localized SH bond orbital in the bridge, as shown in **9c**. This orbital is directed toward the p orbital of the Cl^- in the second X position. This enlarged SH_2–Cl^- interaction in the bridge is responsible for the stabilization of **9c** compared to **8c**.

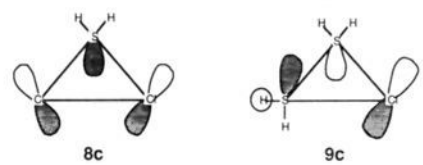

For the $2a_1$ orbital of VIIIa, where three sulfur ligands are forming the bridge, we find that these SH bond orbitals for both sulfur systems are pointing directly toward each other, as shown in **10**. This strong bonding sulfur–sulfur interaction causes

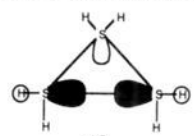

(75) Boorman, P. M.; Gao, X.; Freeman, G. K. W.; Fait, J. F. *J. Chem. Soc., Dalton Trans.* **1991**, 115.

(76) Boorman, P. M.; Gao, X.; Fait, J. F.; Parvez, M. *Inorg. Chem.* **1991**, *30*, 3886.

Scheme II

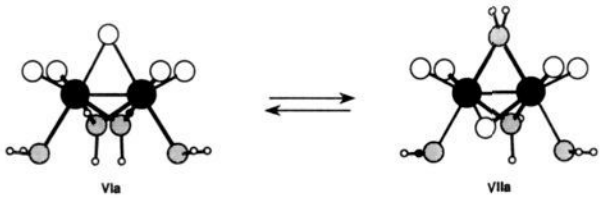

additional stabilization of the $2a_1$ orbital. It seems that in systems with two thioethers in X position, a partial, localized bond between these two ligands is formed. Strong sulfur–sulfur interactions, resulting in short sulfur–sulfur separations, are well known for thiolato-bridged complexes.[79,80] For tungsten systems bridged by more than one thioether, the sulfur–sulfur separation is also well within the accepted van der Waals radius of 370 pm.[28,81,82]

It should be mentioned that this analysis only applies to the relative changes in the electronic structure. Nothing has been said about the relative stabilities of the different systems. As discussed in the previous section, steric influences will be of major importance for the overall bonding energy.

Finally, we will include into our discussion VIa, a compound with two thioethers in the X position but none in the Y position. Based on our inspections which we made so far, we can easily predict the changes in the electronic structure for the isomerization reaction $(SH_2)Cl_2Mo(\mu\text{-}SH_2)(\mu\text{-}Cl)(\mu\text{-}SH_2)MoCl(SH_2)_2$ (VIIa) ↔ $(SH_2)Cl_2M(\mu\text{-}SH_2)_2(\mu\text{-}Cl)MoCl_2(SH_2)$ (VIa) (Scheme II). On going from VIIa to VIa, the 3a′ orbital will turn into the $2a_1$ orbital of lower energy, since we gain energy due to the sulfur–sulfur interaction as discussed above. On the other hand, we lose the back-bonding from the metal fragment, when we move a SH_2 ligand from the Y position into the X position. Therefore, orbital 2a′ will go up in energy to correlate with the $1b_2$ orbital.

Figure 9 displays the energy level diagram for the frontier orbitals of VIIa and VIa. As expected, the energetic levels of $2a_1$ and $1b_2$ for VIa are reversed. The same effect can be seen for the empty orbitals $1a_2$ and $1b_1$. 1a′ remains at almost the same energy to go over into $1a_1$.

It is more difficult to predict whether complex VIa or VIIa is the more stable isomer. We know that the large bonding contributions of a thioether in the Y position is accompanied by an increase of steric repulsion, due to a short metal–ligand bond. We know further that the metal–ligand bond for Cl^- in the Y position is stronger than the corresponding bond with SH_2 in the Y position. Therefore, one might expect VIa to be the more stable compound.

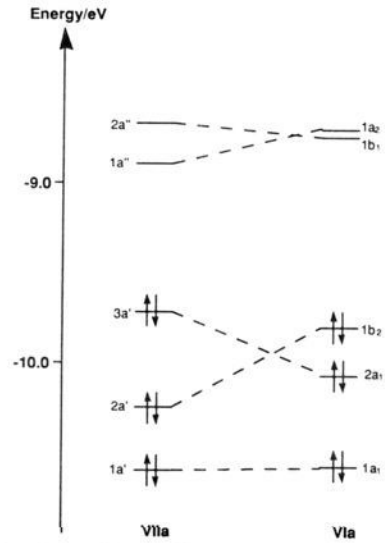

Figure 9. Correlation diagram for the isomerization reaction between $(SH_2)Cl_2Mo(\mu\text{-}SH_2)(\mu\text{-}Cl)(\mu\text{-}SH_2)MoCl_2(SH_2)$ (VIIa) and $(SH_2)Cl_2Mo(\mu\text{-}SH_2)_2(\mu\text{-}Cl)MoCl_2(SH_2)$ (VIIa).

The calculations shows that this is indeed the case. The isomerization energy for this process is calculated to be 22.1 kJ/mol. The complexes VIa and VIIa are close in energy and VIa is thermodynamically favored.

4. Summary and Conclusions

We have demonstrated that density functional theory[13] is able to account quantitatively for the fine balance between metal–metal bonding and metal–ligand bonding interactions in bridged binuclear complexes with respect to different ligands. Our main objective in the present investigation has been to elucidate the bonding of thioethers to the metal centers in d^3–d^3 Mo–Mo bioctahedral frameworks. We have found that thioethers in general have to be seen as good σ donors. In contrast to common belief, the orbital on the thioether responsible for back-bonding is not an empty d orbital on the sulfur, but rather, as is the case for phosphines, it is a low-lying σ^* orbital of the thioether that accepts electron density from the metal center. For the special case of our bioctahedral molecules, the π acceptance is greater for thioethers in the bridging position. The variation in donor and acceptor strength exhibits the expected influence of the substituent on the thioether. The bridging position is generally the preferred position, as it has been demonstrated by the calculation of the ligand isomerization process $thioether_{terminal}$ (IIa) versus $thioether_{bridging}$ (IIIa). The isomerization is accompanied by a significant shortening of the Mo–Mo bond, due to a decrease in repulsion for the bridging region of the bioctahedron. Further work is under way addressing the question of π-acceptor strength, making use of the comparison with known π acceptors.

Acknowledgment. This investigation was supported by the Natural Sciences and Engineering Research Council of Canada (NSERC). We thank Professor E. J. Baerends and Professor W. Ravenek for a copy of their vectorized LCAO–HFS program system and the University of Calgary for access to their IBM-6000-RISC facilities.

(77) Benson, I. B.; Knox, S. A. R.; Naish, P. J.; Welch, A. J. *J. Chem. Soc., Chem. Commun.* **1978**, 878.
(78) Weidenhammer, K.; Ziegler, M. L. *Z. Anorg. Allg. Chem.* **1979**, *422*, 29.
(79) Stiefel, E. I.; Miller, K. F.; Bruce, A. E.; Corbin, J. L.; Berg, J. M.; Hodgson, K. O. *J. Am. Chem. Soc.* **1980**, *102*, 3624.
(80) Boorman, P. M.; Codding, P. W.; Kerr, K. A.; Moynihan, K. J.; Patel, V. A. *Can. J. Chem.* **1982**, *60*, 1333.
(81) Moynihan, K. J. Ph.D. Thesis, University of Calgary, Calgary, Alberta, Canada, 1983.
(82) Gao, X. Private communication.
(83) Dahl, J. P., Avery, J., Eds. *Local Density Approximations in Quantum Chemistry and Solid State Physics*, Plenum Press: New York, 1984.
(84) Parr, R. G.; Yang, W. *Density Functional Theory of Atoms and Molecules*; Oxford University Press: New York, 1989.